

Identification of biochemical pathways for the metabolism of oxidized low-density lipoprotein derived aldehyde-4-hydroxy *trans*-2-nonenal in vascular smooth muscle cells

Sanjay Srivastava ^a, Daniel J. Conklin ^b, Si-Qi Liu ^a, Nidhi Prakash ^c, Paul J. Boor ^d,
Satish K. Srivastava ^c, Aruni Bhatnagar ^{a,*}

^a Experimental Research Laboratories, Division of Cardiology, University of Louisville, and Jewish Hospital Heart and Lung Institute, Louisville, KY 40202, USA

^b Department of Biology, University of Wisconsin Eau Claire, Eau Claire, WI 54702-4004, USA

^c Department of Human Biological Chemistry and Genetics, University of Texas Medical Branch, Galveston, TX 77555-0647, USA

^d Department of Pathology, University of Texas Medical Branch, Galveston, TX 77555-0647, USA

Received 1 June 2000; received in revised form 12 October 2000; accepted 24 January 2001

Abstract

Oxidation of low-density lipoproteins (LDL) generates high concentrations of unsaturated aldehydes, such as 4-hydroxy *trans*-2-nonenal (HNE). These aldehydes are mitogenic to vascular smooth muscle cells and sustain a vascular inflammation. Nevertheless, the processes that mediate and regulate the vascular metabolism of these aldehydes have not been examined. In this communication, we report the identification of the major metabolic pathways and products of [³H]-HNE in rat aortic smooth muscle cells in culture. High-performance liquid chromatography separation of the radioactivity recovered from these cells revealed that a large (60–65%) proportion of the metabolism was linked to glutathione (GSH). Electrospray mass spectrometry showed that glutathionyl-1,4 dihydroxynonene (GS-DHN) was the major metabolite of HNE in these cells. The formation of GS-DHN appears to be due aldose reductase (AR)-catalyzed reduction of glutathionyl 4-hydroxynonanal (GS-HNE), since inhibitors of AR (tolrestat or sorbinil) prevented GS-DHN formation, and increased the fraction of the glutathione conjugate remaining as GS-HNE. Gas chromatography–chemical ionization mass spectroscopy of the metabolites identified a subsidiary route of HNE metabolism leading to the formation of 4-hydroxynonanoic acid (HNA). Oxidation to HNA accounted for 25–30% of HNE metabolism. The formation of HNA was inhibited by cyanamide, indicating that the acid is derived from an aldehyde dehydrogenase (ALDH)-catalyzed pathway. The overall rate of HNE metabolism was insensitive to inhibition of AR or ALDH, although inhibition of HNA formation by cyanamide led to a corresponding increase in the fraction of HNE metabolized by the GSH-linked pathway, indicating that ALDH-catalyzed oxidation competes with glutathione conjugation. These metabolic pathways may be the key regulators of the vascular effects of HNE and oxidized LDL. © 2001 Elsevier Science Ireland Ltd. All rights reserved.

Keywords: Lipid peroxidation; 4-Hydroxy-*trans*-2-nonenal; Glutathione conjugates; Aldose reductase; Vascular smooth muscle cells; Atherosclerosis

1. Introduction

High concentrations of unsaturated aldehydes such as 4-hydroxy *trans*-2-nonenal (HNE), malonaldehyde (MDA) and acrolein [1–3] are generated during in vitro oxidation of low-density lipoprotein (LDL). These aldehydes form covalent adducts with apolipoprotein (apo) B [1,2,4–6], and trigger the uptake of LDL by scavenger receptors [6] located on vascular tissues, including

* Corresponding author. Present address: Division of Cardiology, Jewish Cardiovascular Research Center, 500 South Floyd Street, University of Louisville, Louisville, KY 40202, USA. Tel.: +1-502-8524883; fax: +1-502-8521795.

E-mail address: aruni@louisville.edu (A. Bhatnagar).

vascular small muscle cells (VSMC) [1,6]. Moreover, antibodies against protein–HNE and protein–MDA adducts stain atherosclerotic lesions [6–9], and high titers of these antibodies are present in sera of human and animals with peripheral or coronary artery disease and in apoE-deficient mice [10–12]. The aldehydes generated during oxidation do not remain sequestered in the LDL particle, but diffuse to distal sites [13] generating epitopes that do not colocalize with apoB [6]. In addition, antibodies against protein aldehyde adducts also stain focal areas of neointima after balloon injury [14], and VSMC of arteries with giant cell arteritis [15]; and increased formation of lipoxidation products such as HNE and MDA has been reported for diabetic aorta [16]. Nevertheless, the contribution of these aldehydes to atherogenesis remains unclear.

The α,β -unsaturated aldehydes (alkenals and 4-hydroxyalkenals) are derived from the oxidation of ω -6-polyunsaturated fatty acids such as arachidonic, linolenic and linoleic acids [2], which are particularly abundant in LDL [17]. Due to the conjugated α,β -unsaturation, these aldehydes react avidly with cellular nucleophiles such as glutathione, cysteine, lysine and histidine side chains of proteins, and with DNA bases [2]. As a result, high concentrations of these aldehydes are cytotoxic to most cells, and non-cytotoxic concentrations cause profound changes in gene expression and cellular metabolism. The HNE, for instance, stimulates VSMC growth [18], and forms selective adducts with c-Jun N-terminal kinase, inducing its phosphorylation [19]. It also increases DNA binding activity of AP-1 [18,20], production of reactive oxygen species (ROS) [20], and transforming growth factor- β [21], and inhibits the NF- κ B/Rel system and the synthesis of tumor necrosis factor (TNF)- α [22]. These observations suggest that low steady-state generation of lipid-derived aldehydes mediates and sustains chronic inflammation. Indeed, it has been proposed that these aldehydes act as second messengers of ROS [2] to signal or indicate pro-oxidant states.

To understand how aldehydes derived from oxLDL regulate and alter VSMC function, it is essential to identify the processes involved in their metabolism and detoxification. However, little is known in regard to the mechanisms by which VSMC metabolize these aldehydes. The present study was, therefore, designed to identify the major biochemical pathways involved in the VSMC metabolism of HNE, which is one of the most abundant and toxic aldehydes generated during the oxidation of LDL [1,2].

2. Materials

Cyanamide, 4-methyl pyrazole (4-MP), aldehyde dehydrogenase (ALDH), NAD, NADPH and glutathione

(GSH) were purchased from Sigma Chemical Company. Sorbinil (CP-45643; (+)-(4*S*)-6-fluorospiro(chroman-4,4'-imidazolidine)-2,5'-dione) and tolrestat (Ay-27773; *N*-[6-methoxy-5-(trifluoromethyl)-1-naphthalenyl]thioxomethyl-glycine) were gifts from Pfizer and Ayerst, respectively. All other reagents were of the highest purity available.

3. Methods

3.1. Chemical synthesis

[4-³H]-HNE was synthesized as its dimethyl acetal with a specific activity of 75–100 mCi/mmol as described earlier [23]. Prior to the experiments, [³H]-HNE was released by the acid hydrolysis of the dimethyl acetal and purified by high-performance liquid chromatography (HPLC). Radiolabeled 1,4-dihydroxy-2-nonenone (DHN), 4-hydroxy-2-nonenic acid (HNA), glutathionyl conjugate of HNE (GS-HNE) and its reduced form (GS-DHN) were synthesized using recombinant aldose reductase (AR) as described earlier [24] and purified by HPLC. The identity and purity of the reagent HNE, DHN and HNA were established by nuclear magnetic spectroscopy and gas chromatography–chemical ionization mass spectroscopy (GC–CI/MS), and that of GS-HNE and GS-DHN by electrospray ionization mass spectroscopy (ESI/MS).

3.2. HPLC analysis

Synthesized radiolabeled standards were separated by HPLC using a Varian ODS C₁₈ column pre-equilibrated with 0.1% trifluoroacetic acid at a flow rate of 1 ml/min. The gradient was established such that *B* reached 16.6% in 20 min, 41.5% in 35 min and held at 41.5% for 30 min. In an additional 10 min, *B* reached 100% and was held at this value for 20 min. In this system, the retention time (τ_R) of the glutathione conjugates (GS-HNE and GS-DHN) was 46 min, and the DHN, HNA and HNE eluted at $\tau_R = 59, 68, \text{ and } 76$ min, respectively (Fig. 1A).

3.3. Mass spectrometry

ESI/MS analyses were performed on a Finnigan MAT TSQ70 triple quadrupole instrument upgraded with TSQ 700 software and a 20-kV conversion dynode electron multiplier. The ESI/MS operating parameters were as follows: needle voltage, 3.6 kV; nozzle voltage, 250 V; repeller voltage, 5 V; and source block temperature, 155°C. Wherever required, bath nitrogen was introduced into the spray region at 3 psi. Samples were diluted 1:5 with the solvent (100/100/0.5 (v/v), methanol/water/acetic acid) and then introduced into

the mass spectrophotometer using a Harvard syringe pump at a rate of 0.82 $\mu\text{l}/\text{min}$. Spectra were acquired at the rate of 275 atomic mass units/s over the range 100–650 atomic mass units.

3.4. Gas chromatography–chemical ionization mass spectrometry

For GC–CI/MS analyses, the samples were derivatized with 10 μl diethyl ether and 50 μl *N*-methyl-*N*-(τ -

butyldimethylsilyl)-trifluoroacetamide for 40 min at room temperature. One microliter aliquots were used for analysis. The GC–CI/MS analysis was performed using a Finnigan Incos 50 GC/MS system held at a temperature of 150°C using ammonia as the reagent gas. Gas chromatographic separation was achieved using a DB-5 fused silica capillary column (30 m \times 0.32 mm inside diameter, 0.25 μm film thickness; J&W Scientific, Folson, CA). The column was held at 115°C for 5 min, and then programmed to increase at a rate of 4°C/min to 165°C, and then to 250°C at a rate of 50°C/min. The column was held at 250°C for 5 min. Other parameters were: injector temperature, 270°C; and transfer line temperature, 280°C. To avoid a large peak due to the *N*-methyl-*N*-(τ -butyldimethylsilyl)-trifluoroacetamide reagent, chemical ionization mass spectra were collected in the positive ion mode over a range from m/z 245 to 500 at a rate of 1 scan/s.

3.5. Isolation and culture of VSMC

Cells were dissociated enzymatically from the aortae of male Sprague–Dawley rats (200–300 g; Harlan, Indianapolis, IN). Purity of the isolated VSMC was established by immunohistochemistry using smooth muscle α -actin and Factor VIII antibodies. Cells were seeded and grown in T75 flasks (Corning, VWR, Houston, TX) in Dulbecco's Modified Eagle Medium (Gibco BRL, Grand Island, NY) supplemented with 10%, heat-inactivated bovine fetal calf serum (Hyclone, Logan, UT) and 0.1% penicillin/streptomycin. Two different preparations of cells from passage 6–13 were used for these studies. After serial passaging, most rat VSMC are of the synthetic phenotype [25]. The cells were seeded at a density of 2×10^6 cells per T-75 flask. The cells became confluent in 4–5 days, reaching a density of $(8–10) \times 10^6$ cells per flask. Cell viability was determined by the enzyme-linked immunosorbent assay-based 3-(4,5-dimethyl thiazol-2-yl)-2,5-diphenyl tetrazolium (MTT) assay (Roche Diagnostics, Indianapolis, IN).

3.6. Metabolic studies

Initial experiments described the time course of HNE metabolism. VSMC grown in T75 flasks were incubated in 9 ml pre-warmed (37°C) modified KH buffer, containing (in mM/l): NaCl, 118; KCl, 4.7; MgCl₂, 1.25; CaCl₂, 3.0; KH₂PO₄, 1.25; ethylenediamine tetraacetic acid, 0.5; NaHCO₃, 25; and glucose, 10; pH 7.4. Pre-warmed (37°C) KH buffer had no observable effect on VSMC viability for the duration of the experiment. The incubation was started with the addition of 50 nmol [³H]-HNE in 1.0 ml KH buffer. Aliquots were with-

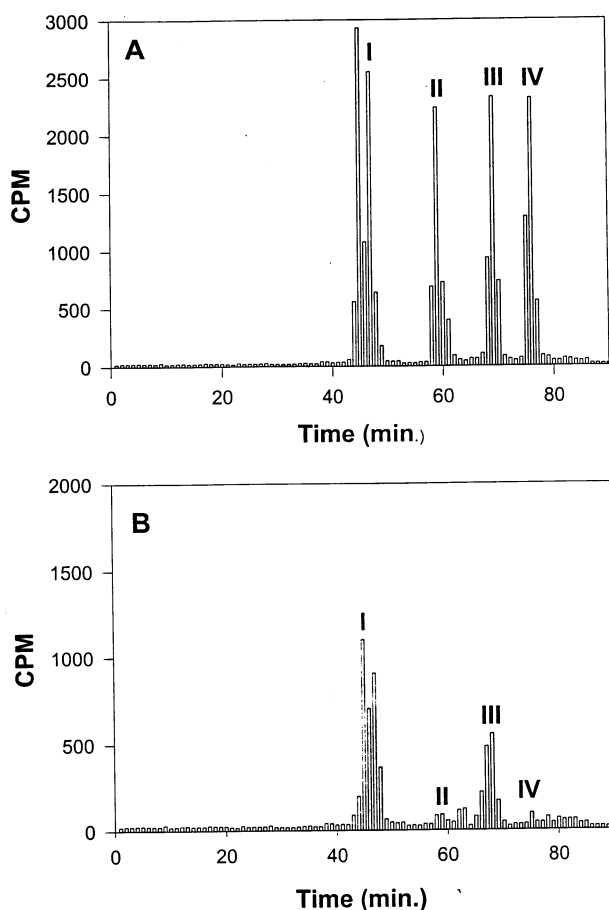


Fig. 1. (A) HPLC profile of synthesized putative metabolites of [³H]-HNE. Tritiated HNE, DHN, HNA, GS-HNE and GS-DHN were synthesized as described in Section 2. Each metabolite containing approximately 5000 cpm (\approx 5 nmol) was diluted to 2 ml with KH buffer and applied to ODS C₁₈ reverse-phase HPLC column. One milliliter fractions of the eluate were collected every min and radioactivity was measured in each fraction. Retention time (τ_R) was found to be 46 min for the glutathione conjugates (GS-HNE and GS-DHN peak I), 59 min for DHN (peak II), 68 min for HNA (peak III) and 76 min for HNE (peak IV). (B) HPLC profile of radiolabeled metabolites of [³H]-HNE collected from VSMC. The VSMC were incubated with 50 nmol [³H]-HNE in 5.0 ml KH buffer. After 30 min at 37°C, the KH buffer was collected, centrifuged at $10\,000 \times g$ for 10 min, and ultrafiltered. The radioactivity collected in the medium was measured and separated by HPLC using an ODS C₁₈ column. Radioactivity in the HPLC eluate was measured in 1 ml fractions. Peaks I–IV are marked: peak I corresponds to the reagent glutathione conjugates of HNE, whereas peaks II, III and IV correspond to DHN, HNA and unmetabolized HNE, respectively.

Table 1
Percent distribution of metabolites recovered in the medium from vascular smooth muscle cells incubated with [³H]-HNE^a

	Peak I (glutathione conjugates)	Peak II (DHN)	Peak III (HNA)	Peak IV (HNE)	Others
<i>HNE</i>					
5 Min	63	3	11	20	3
10 Min	67	3	13	11	6
20 Min	64	3	23	4	6
30 Min	65	3	28	1	3
<i>HNE+Sorbinil</i>					
5 Min	64	3	11	19	3
10 Min	60	6	14	12	8
20 Min	66	2	24	5	3
30 Min	63	3	27	2	5

^a Vascular smooth muscle cells (1.0×10^7) were incubated with 5 nmol [³H]-HNE, and the metabolites present in the incubation media were separated by HPLC as described in the text. The results are given as percentage of the total radioactivity recovered from HPLC.

drawn at indicated times, centrifuged at $10\,000 \times g$ for 10 min at 4°C, and the supernatant was ultrafiltered and applied to Varian ODS C₁₈ reverse-phase column. The metabolites of [³H]-HNE were determined by quantifying the radioactivity in each fraction. Individual peaks were analyzed by ESI/MS or GC–CI/MS.

4. Results

4.1. HNE consumption

To examine HNE metabolism, T-75 flasks containing VSMC were used. The culture medium was removed and the cells were incubated with 5 or 10 μM [³H]-HNE in 10 ml KH buffer. Incubation of the cells with 5 or 10 μM HNE for 6 h did not cause a significant change in cell viability as determined by the MTT assay. For measuring the rate of HNE metabolism, aliquots were withdrawn at various times and the radioactivity in the medium was separated by HPLC. HNE remaining in the medium was determined by measuring radioactivity in the peak eluting with a retention time (τ_R) of the reagent HNE (76 min; Fig. 1A). As shown in Table 1, $\geq 80\%$ of HNE was metabolized in 5 min. After 30 min of incubation, only 1–2% unmetabolized HNE remained in the medium. The total radioactivity recovered from the incubation medium was $80 \pm 7\%$; $\leq 1\%$ radioactivity was recovered from the acid-insoluble

fraction after 30 min of incubation. Analysis of the rate of consumption of HNE using a monoexponential decay function showed that the half-life of HNE in the medium was approximately 2.4 min. The rate of HNE consumption was calculated to be 7.3 nmol/mg protein/min. Upon HPLC separation of the medium, individual peaks were assigned to specific HNE metabolites (Fig. 1) on the basis of τ_R of the synthesized standards. As shown in Table 1, after 5 min of incubation, 63% of the radioactivity in the medium was present as glutathione conjugates. Upon further incubation, the relative radioactivity recovered as glutathione conjugates did not change, and most of the residual HNE consumption was accounted for by the formation of HNA. Thus, conjugation with glutathione appears to be a rapid, high-affinity route of HNE elimination, whereas direct oxidation of HNE appears to be a slower process that competes with the glutathione-linked metabolism.

Because the τ_R of Peak I of the HNE-treated VSMC was identical to reagent glutathionyl conjugates, fractions corresponding to this peak were subjected to ESI⁺/MS in order to characterize the metabolite(s) present. To identify the glutathione conjugates, putative conjugates were synthesized and analyzed by ESI⁺/MS. The ESI⁺ mass spectrum of the reagent GS-HNE showed a molecular ion $[M + H]^+$ with a m/z of 464 (Fig. 2A). Additional species with m/z 446 and 455 were ascribed to daughter ions arising from the loss of a single water molecule from the parent 464 ion, and

Fig. 2. The ESI⁺ mass spectrum of reagent GS-HNE and GS-DHN. Glutathione conjugates of HNE and DHN were synthesized and purified on HPLC and injected into electrospray as described in Section 2. (A) Spectrum of GS-HNE: the species with a m/z value of 464.22 was assigned to the parent ion, whereas species with m/z values of 446.23 and 455.15 appear to be due to daughter ions originating from in-source dehydration of the parent ion. (B) Spectrum of GS-DHN: the parent ion forms a well-resolved ion with m/z 466.02. Subsidiary peaks with m/z values of 456.05 and 446.07 appear to be due to dehydration of GS-DHN, and residual GS-HNE in the reaction mixture, respectively. (C) The ESI⁺ mass spectrum of HNE metabolites eluting as Peak I on HPLC separation. The VSMC were incubated with 50 nmol [³H]-HNE in 5.0 ml KH buffer for 30 min at 37°C. The radioactivity in the medium was separated by HPLC, and fractions corresponding to Peak I were pooled and injected into the electrospray. The major species with a m/z value of 466.20 was assigned to $[M + H]^+$ of GS-DHN. The molecular ions with m/z values of 307.2 and 446 are due to $[M + H]^+$ of GSH and dehydrated GS-HNE, respectively, whereas the species with a m/z value of 317.34 corresponds to $[M + H]^+$ of dehydrated Gly-Cys-HNE.

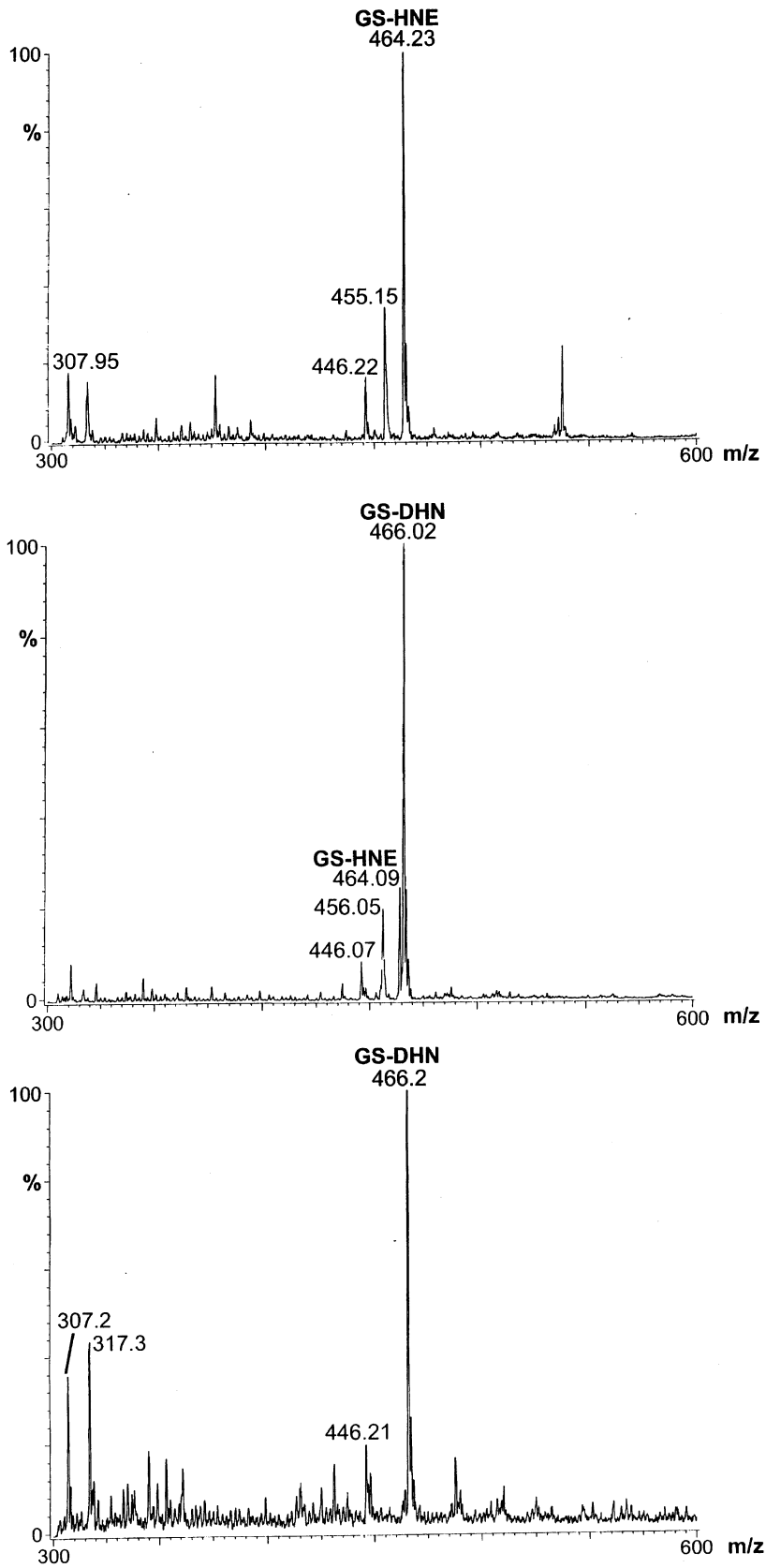


Fig. 2.

due to the dehydration of the GS-HNE dimer ($(464 \times 2) - 18/2$), respectively, because the 446 and 455 species could be completely converted at lower cone voltages to the 464 species. The ESI⁺ mass spectrum of reagent GS-DHN displayed a single pseudo-molecular ion $[M + H]^+$ with a m/z value of 466. No daughter ions due to dehydration of the parent ion were observed (Fig. 2B). Peaks with m/z values of 464, 456, and 446 are due to non-reduced GS-HNE.

The ESI⁺ mass spectrum of Peak I showed a predominant peak at m/z 466.2, which was assigned to the +1 charge state of GS-DHN (Fig. 2). Additional peaks with m/z values of 307.2 and 317.3 were also detected. These corresponded to 36 and 44% of the GS-DHN signal. Assuming a singly charged species, these peaks were assigned to GSH and Gly-Cys-HNE (desglutamyl GS-HNE). There was a small signal with a m/z value of 446.2 that, on the basis of a similar peak observed with reagent GS-HNE, was ascribed to dehydrated GS-HNE [M-18]. This peak represents 20% of the GS-DHN signal. From the 466 and the 446 peaks, the ratio of GS-DHN to GS-HNE was calculated to be 8.0, indicating that the extruded conjugate is predominantly GS-DHN. The τ_R of Peak II, which accounted for 3% of the total radioactivity, corresponded to the τ_R of reagent DHN. An addition peak, eluting at $\tau_R = 62$ min, accounted for 4% of the radioactivity. This peak was not further analyzed.

The τ_R of Peak III, which represents 28% of the total radioactivity, was identical to reagent HNA (Fig. 1). To characterize this peak further, fractions corresponding to this peak were pooled, sililated and subjected to GC-MS. The gas chromatograph (Fig. 3A) shows a prominent solvent-independent peak with a τ_R value identical to reagent HNA. This peak was further subjected to MS analysis. As shown in Fig. 3B, a molecular ion with a m/z value of 401.3, corresponding to derivatized HNA, was observed. The fragmentation pattern of this ion was found to be identical to that of synthetic HNA (data not shown), indicating that peak III is due to HNA. The peak IV displayed high absorbance at 224 nm and appears to be due to the unmetabolized HNE, since it eluted with a τ_R value identical to reagent HNE (76 min).

4.2. Identification of the metabolic pathway

The HPLC and mass spectroscopic analyses already described clearly demonstrate that the major metabolic products of HNE in VSMC are GS-HNE, GS-DHN and HNA. To identify the biochemical pathways involved in the formation of these metabolites, the VSMC were incubated for 1 h at 37°C with inhibitors of AR (sorbinil, 200 μ M or tolrestat, 10 μ M), alcohol dehydrogenase (4-MP, 400 μ M), or ALDH (cyanamide,

2 mM) in 5 ml KH buffer, after which 50 nmol [³H]-HNE were added to the medium, and the incubation was continued for an additional 30 min. Cells incubated with KH buffer under identical conditions served as control. Incubation of the VSMC with 5.0 μ M HNE, with or without these inhibitors for 6 h, did not significantly affect cell viability as determined by the MTT assay.

Radioactivity in the incubation medium of sorbinil-treated VSMC separated into four peaks on HPLC (Table 2). A total of $58 \pm 9\%$ radioactivity was recovered in Peak I, with a τ_R value corresponding to glutathione conjugates, whereas Peak III with a τ_R value corresponding to HNA accounted for $26 \pm 4\%$ of the total radioactivity recovered in the incubation medium. The ESI⁺ mass spectrum of peak I obtained from sorbinil-treated cells shows prominent ions with a m/z value of 466 corresponding to $[M + H]^+$ of GS-DHN, 464.07 corresponding to $[M + H]^+$ of GS-HNE, and 446.26 corresponding to the dehydrated [M-18] daughter ion of GS-HNE, respectively. Together, the ions due to GS-HNE accounted for a signal roughly equivalent to that due to GS-DHN. From these data, we infer that sorbinil significantly inhibits the reduction of GS-HNE in VSMC (compare Fig. 4A,B). To confirm the role of AR in the reduction of GS-HNE in VSMC further, we examined the effect of another, structurally different, AR inhibitor — tolrestat [26]. The HPLC elution profile of the HNE metabolites of tolrestat-treated VSMC was similar to that obtained with sorbinil-treated cells (Table 2). Moreover, similar to the sorbinil-treated cells, the ESI⁺ mass spectrum of peak I of the metabolites obtained from the incubation medium of the tolrestat-treated cells shows strong signals corresponding to the molecular ions of GS-HNE and GS-DHN (Fig. 4C). The ion with a m/z ratio of 456.19 was also assigned to GS-HNE, since a similar peak was observed with reagent GS-HNE, presumably due to dehydration of the GS-HNE dimer. The relative abundance of the GS-HNE:GS-DHN in the tolrestat-treated cells was roughly 1.5. Thus, treatment of VSMC with two structurally unrelated inhibitors of AR, sorbinil and tolrestat significantly inhibits the reduction of GS-HNE.

In addition to AR, we also examined the possible involvement of alcohol dehydrogenase (ADH) in the reduction of GS-HNE in VSMC, because ADH has been reported to catalyze the reduction of HNE in hepatocytes [2]. However, incubation of VSMC with the ADH inhibitor 4-MP did not inhibit the reduction of GS-HNE to GS-DHN in VSMC (Fig. 4D), indicating that reduction of glutathionyl conjugate of HNE is not catalyzed by ADH in these cells. The metabolism of HNE in VSMC was, however, significantly perturbed by the ALDH inhibitor, cyanamide. The radioactivity

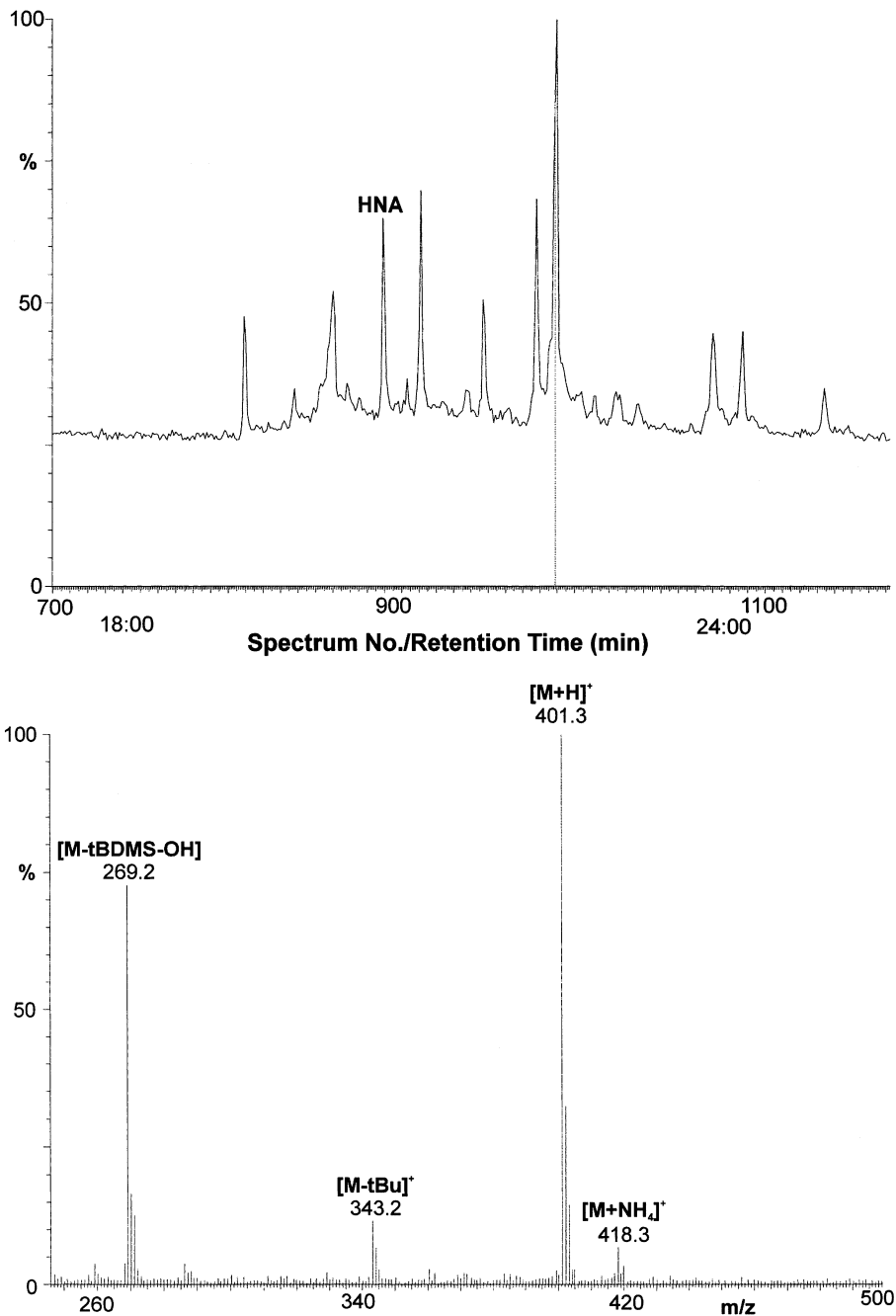


Fig. 3. The GC–CI mass spectrum of Peak III obtained from HPLC separation of tritiated metabolites extruded by the VSMCs treated with [^3H]-HNE. Fractions corresponding to peak IV were pooled, derivatized and subjected to GC–CI. (A) Typical gas chromatogram of Peak III. The peak with the retention time of reagent HNA is marked. The positive ionization mass spectrum is shown in (B). The parent ion displayed a m/z value of 401.3, with indicated derivatives of m/z values of 269.2, 343.2 and 418.3.

in Peak IV corresponding to HNA decreased by $64 \pm 4\%$ in cells pre-incubated with cyanamide as compared with those treated with [^3H]-HNE alone (Table 2). In addition, the radioactivity present in Peak I, which contained the glutathione conjugates, increased by $26 \pm 3\%$. Based on these observations, we infer that the formation of HNA is catalyzed by ALDH, and that

inhibition of HNA formation leads to a corresponding increase in the glutathione-linked metabolism. The ESI $^+$ mass spectrum of Peak I showed that cyanamide had no significant effect on the GS-HNE:GS-DHNE ratio (data not shown), suggesting that inhibition of ALDH does not perturb the reduction of the glutathione conjugate.

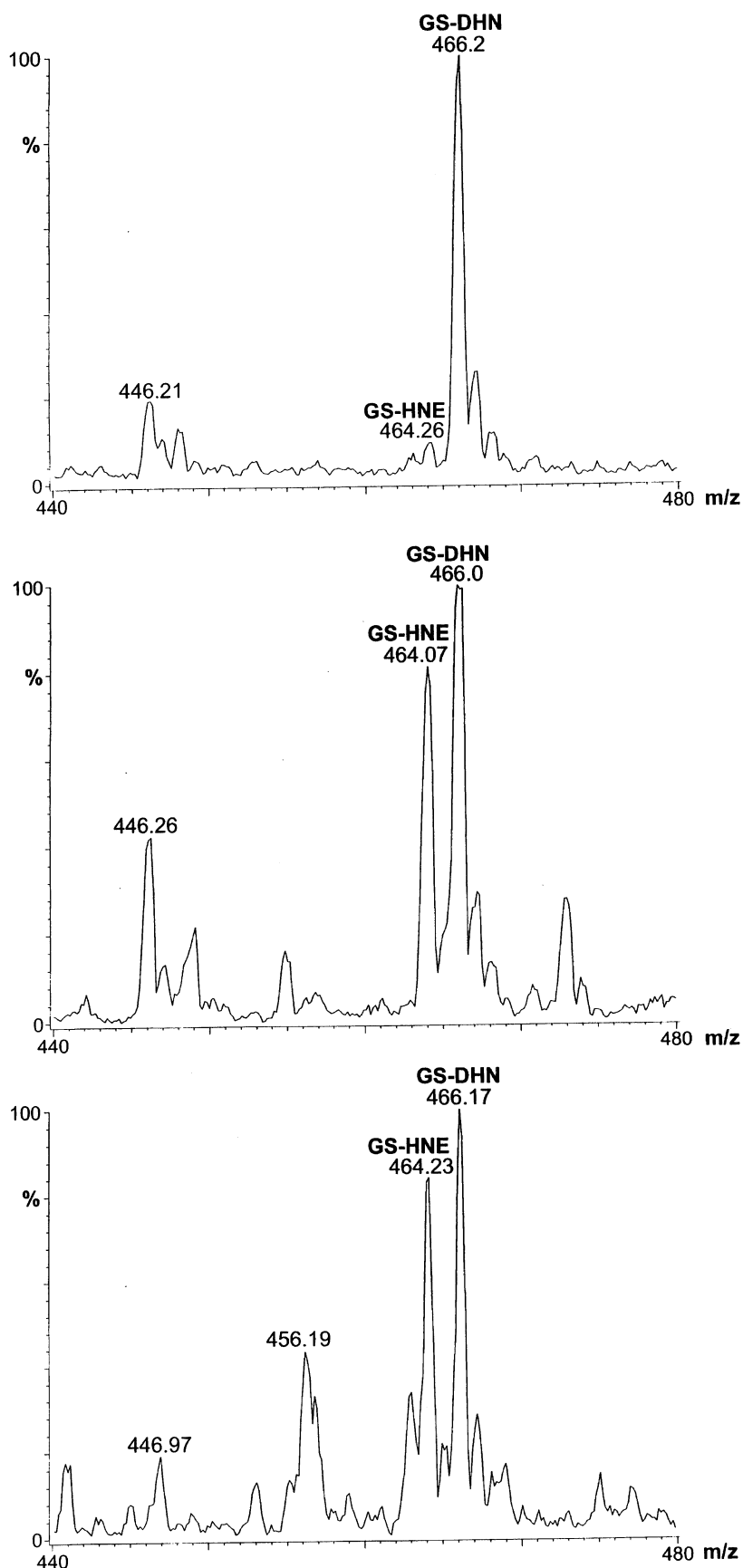


Fig. 4. The effect of aldose reductase aldehyde dehydrogenase inhibitors on HNE metabolism. The VSMC were incubated with sorbinil or tolrestat in 4 ml KH buffer for 1 h at 37°C, after which 1 ml KH buffer containing 50 nmol [3 H]-HNE was added to the incubation media, and the flasks were incubated for an additional 30 min. Metabolites in the media were separated on HPLC and fractions corresponding to Peak I were analyzed by ESI $^+$ /MS. (A) Control (untreated cells), and cells treated with (B) 200 μ M sorbinil, (C) 10 μ M tolrestat, and (D) 400 μ M 4-methyl pyroazole.

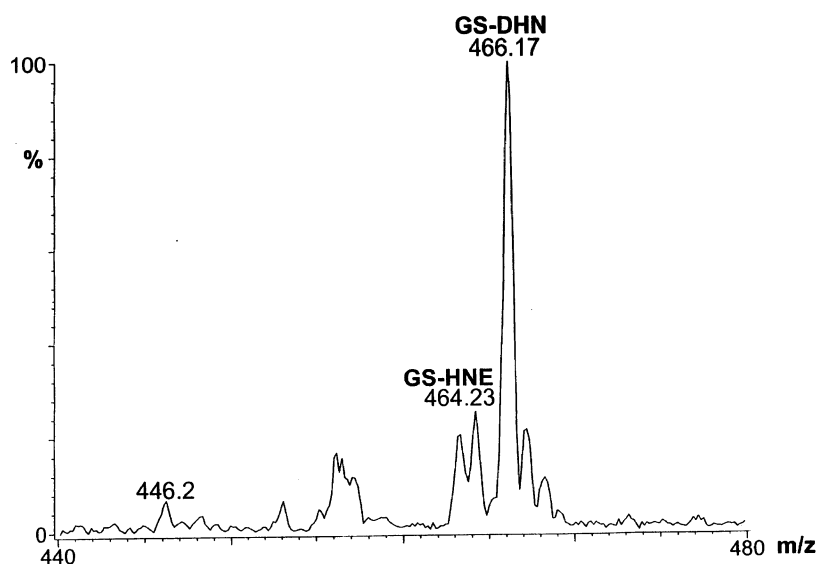


Fig. 4. (Continued)

5. Discussion

Despite extensive evidence implicating oxLDL and its products in regulating VSMC growth and function, the mechanisms by which these oxidants affect VSMC are not well understood. The observations that oxidation of LDL increases the formation of lipid-derived aldehydes [1–3] suggest that the generation and metabolism of these aldehydes may be an important determinant of the VSMC redox state. Surprisingly, little is known of the mechanism by which VSMC metabolize these aldehydes although their metabolism in tissues such as the heart [24] and liver [2] has been studied. An understanding of VSMC-specific metabolism is, however, a prerequisite for assessing the oxidative effects of oxLDL on vascular pathophysiology.

Our studies show that HNE is extensively transformed by VSMC to several metabolites. Generation of multiple products is a characteristic of the metabolism of lipid-derived aldehydes [2]. This is in contrast to the metabolism of ROS, such as superoxide and peroxides, which are predominantly detoxified via a single high-affinity, high-capacity pathway (although compensatory

pathways exist as back-ups to the primary defenses, these yield non-unique products). Measurements of the rate of consumption of HNE show that it is rapidly metabolized and extruded to the medium such that < 1% of the radioactivity remained covalently bound to cell constituents. Thus, previous immunological measurements of the adduct of lipid peroxidation-derived aldehydes, such as HNE with proteins, under the conditions of oxidative stress such as in atherosclerotic vessels are likely to be gross underestimates of the true extent of total aldehyde generation. Even measurement of free lipid derived aldehydes are likely to be underestimates since only a small fraction of the aldehyde appears to escape cellular metabolism. Should a similar metabolic efficiency exist in vivo, the extent of aldehyde generation may be approximately tenfold higher than estimated from the immunoreactivity of protein–aldehyde adducts or measurements of free aldehydes. Although we found that HNE was extensively metabolized, the rate of HNE utilization by VSMC was considerably slower than in other cells. Isolated hepatocytes and enterocytes utilize 25–28 nM HNE/mg wet weight/min [27], which is approximately 100-fold higher

Table 2
Role of oxidoreductases in HNE metabolism in vascular smooth muscle cells^a

Additives	Peak I (glutathione conjugates)	Peak II (DHN)	Peak III (HNA)	Peak IV (HNE)	Others
None (<i>n</i> = 6)	60 ± 8	3 ± 3	28 ± 3	2 ± 2	7 ± 3
Sorbinil (200 μM) (<i>n</i> = 4)	58 ± 9	3 ± 3	26 ± 4	4 ± 1	9 ± 4
Tolrestat (10 μM) (<i>n</i> = 3)	58 ± 5	4 ± 1	25 ± 3	4 ± 2	9 ± 5
4-MP (400 μM) (<i>n</i> = 3)	56 ± 3	4 ± 1	28 ± 2	5 ± 2	7 ± 2
Cyanamide (2 mM) (<i>n</i> = 3)	76 ± 8*	4 ± 2	10 ± 3*	3 ± 3	7 ± 1

^a VSMC were incubated with 50 nmol [³H]-HNE and indicated additives for 30 min at 37°C. At the end of the incubation, the media were collected and separated by HPLC as described in the text. * *P* < 0.05 compared with VSMC incubated with [³H]-HNE without any additives.

than the rate of HNE consumption (7 nM/mg protein/min) measured for VSMC. Whereas a rate of 0.5–2.0 nM/g wet weight/min has been reported for the kidney and heart, respectively [28], these values cannot be directly compared with those obtained with isolated cells, since metabolism in solid tissues is likely to be limited by diffusion. However, in general, the liver appears to possess the highest capacity to metabolize HNE, whereas other tissues such as the heart and kidney are tenfold less efficient [2]. Thus, the HNE metabolizing capacity of VSMC appears to be lower, suggesting that in VSMC the lipid peroxidation products accumulate longer and in higher concentrations than in most other tissues.

Our results show that, in VSMC, 55–60% of the total HNE is metabolized to glutathionyl conjugates. Although it has been shown that HNE and structurally related α,β -unsaturated aldehydes can spontaneously form Michael adducts with glutathione [2], intracellular conjugate formation is thought to be catalyzed by glutathione *S*-transferases (GST) which enhance conjugate formation 300- to 600-fold over the uncatalyzed rate [29]. While several classes of GST isozymes catalyze the conjugation of electrophiles with glutathione, GST 8-8 localized to rat aorta [30] has particularly high specific activity for HNE [31,32] and may be responsible for the high capacity of VSMC to form glutathione conjugates. However, our ESI/MS analysis showed that, in VSMC, the glutathione conjugate of HNE was further metabolized to GS-DHN. This is in contrast to all other cells examined to date, which show either partial [24,33] or no significant reduction [2] of the glutathione conjugate. Because free DHN is not electrophilic, it appears likely that, in VSMC, GS-DHN originates from the enzymatic reduction of GS-HNE rather than spontaneous addition of GSH to DHN. This view is further supported by our observation that incubation of VSMC with [³H]-DHN does not form GS-DHN (data not shown).

Reduction of the glutathionyl conjugate of HNE in VSMC appears to be catalyzed by the polyol pathway enzyme AR, because the formation of GS-DHN was significantly inhibited by two, structurally unrelated, AR inhibitors — sorbinil and tolrestat. Our molecular modeling studies demonstrate that the active site of AR can accommodate the straight-chain lipid peroxidation-derived aldehydes such as HNE as well as their glutathione conjugates [34], and the catalytic efficiency of glutathione–aldehyde conjugates is appreciably higher than the free aldehyde [35,36]. The role of AR in the metabolism of HNE in VSMC is also supported by the observation that exposure of A7r5 cells to HNE enhances the expression of AR [37], and that inhibitors of AR exacerbate long-term HNE toxicity to VSMC [38], enhance the formation of protein–HNE adducts, and

increase inflammation-induced apoptotic cell death *in vivo* [39].

Although *in vitro* AR efficiently catalyzes the reduction of free HNE [34], our observations show that, in VSMC, reduction to DHN accounts for only 3–4% of the total HNE metabolized. It appears likely that the high reactivity of HNE with GSH and the presence of HNE-specific GSTs in the aorta precludes extensive reduction of free HNE by AR, and that, in these and other glutathione competent cells, AR encounters mostly the glutathione conjugate and not the free aldehyde. This is in contrast to other cells such as hepatocytes, in which reduction of free HNE represents 20–30% of the total HNE metabolism [2]. While hepatocytes do not express high levels of AR [40], reduction of HNE in these cells has been suggested to be catalyzed by ADH [2], which presumably has a higher catalytic rate and competes more efficiently with GST than AR. Both ADH I and II efficiently reduce HNE [41]; however, these isozymes are poorly expressed in rat blood vessels [42]. Moreover, the small amount of DHN formed under the present experimental conditions was not inhibited by 4-MP, suggesting that the ADH-catalyzed pathway is not a significant route of HNE metabolism in VSMC.

Besides glutathione-linked metabolism, oxidation of HNE to its carboxylic acid, HNA, represents another major pathway for the biotransformation of HNE in VSMC. The HNA accounted for 25–30% of the total HNE metabolites. The oxidative metabolism of HNE appears to be catalyzed by ALDH, because it was significantly inhibited by the ALDH inhibitor cyanamide. The involvement of ALDH in HNE metabolism has been postulated earlier [2], and it has been shown that ALDH II located in the mitochondrial matrix is particularly effective in oxidizing HNE [43], and may be responsible for the generation of HNA measured in our studies. This pathway of HNE metabolism, however, appears to function in parallel with the glutathione-linked metabolism.

A unique and hereto unrecognized aspect of HNE metabolism revealed by our studies is its insensitivity to inhibition of individual enzymatic pathways. As shown in Tables 1 and 2, the overall rate of HNE consumption was not affected by inhibiting AR or ALDH, suggesting that these metabolic pathways do not control the rate at which HNE is metabolized by VSMC. Indeed, given the high affinity of HNE for GSH and the high concentration of GSH in VSMC [44], it is expected that, even without the 300- to 600-fold acceleration provided by GST, the rate of HNE consumption will be predominantly determined by rate of formation of GS-HNE. Thus, the previously observed protective effects of AR and ALDH [38,39,43] cannot be due to facilitation of HNE removal *per se*. However, it is likely that ALDH (by oxidizing free HNE) diminishes the extent of GS-HNE formation, whereas AR (by converting

GS-HNE to GS-DHN) decreases the time HNE remains in the cell as GS-HNE. The regulation of the extent and duration of GS-HNE formation by AR and ALDH suggests a central role of GS-HNE in regulating the cellular effects of HNE and indicates that GS-HNE is highly reactive. Even though conjugation with glutathione attenuates the reactivity of several electrophiles, it may not be sufficient for detoxification. The GS-acrolein conjugate is markedly nephrotoxic [45] and the glutathione conjugates of 4-hydroxy *trans*-2-hexenal and nonadienal induce DNA damage [46]. These effects have been ascribed partly to the propensity of the glutathione-aldehyde conjugates to generate oxygen free radicals [47]; an effect also observed in intact cells, which show high ROS generation upon exposure to HNE [20]. Thus, reduction of the glutathione-aldehyde conjugate by AR and oxidation of free aldehyde by ALDH may prevent feed-forward amplification of ROS generation by products of lipid peroxidation. Moreover, by reducing the aldehyde, AR may prevent the spontaneous dissociation of GS-HNE, which could deliver the aldehyde to non-exposed sites causing trans-cellular toxicity.

In summary, our results suggest that GST, AR and ALDH-catalyzed pathways are the major biochemical routes for HNE metabolism in VSMC. These pathways of HNE transformation are similar to those present in the heart [24]. Although, the pathophysiological consequences of the multiple metabolites generated from HNE, was not assessed, their effects are likely to be small, because > 80% of the metabolites were extruded from the cells. Nonetheless, further experiments are required to evaluate which, if any, of the metabolites mediate the mitogenic and/or inflammatory effect of HNE. The varied metabolism of HNE has important implications in understanding several pathophysiological effects of oxLDL on VSMC. Because redox changes are associated with mitogenic and cytotoxic effects of oxLDL, this metabolism may be a critical determinant of its cellular effects. Proliferation of VSMC in response to injury is accompanied by increased formation of HNE-protein adducts [14,15] and results in marked upregulation of 'HNE-specific' GST [30] and AR [39]. The expression of AR (and its murine homolog FR-1) is markedly enhanced by mitogens such as FGF, IGF, phorbol esters [48,49] and hydrogen peroxide [38], and under chronic inflammation inhibition of AR leads to apoptosis [39]. Similarly, AR is also stimulated by cytokines such as TNF- α [40] and interferon- γ [39] suggesting that upregulation of aldehyde metabolism is a component of cellular responses to cytokines, which generate oxidants. Thus, based upon the metabolic pathways delineated in the present paper, further studies could be designed to examine how lipid-derived aldehydes, together with the other highly reactive products of lipid peroxidation (e.g. lysophosphatides, oxys-

terols and platelet-activating factor-like substances), affect the VSMC during restenosis and atherosclerosis.

Acknowledgements

This work was supported in part by NIH grants HL55477, HL59378, DK36118, and AHA grant 0060350B. The authors also thank Todd Downes for his help in the preparation of the manuscript and figures.

References

- [1] Witztum JL, Steinberg D. Role of oxidized low density lipoprotein in atherogenesis. *J Clin Invest* 1991;88:1785–92.
- [2] Esterbauer H, Schaur RJ, Zollner H. Chemistry and biochemistry of 4-hydroxynonenal, malonaldehyde and related aldehydes. *Free Radic Biol Med* 1991;11:81–128.
- [3] Uchida K, Kanematsu M, Morimitsu Y, Osawa T, Noguchi N, Niki E. Acrolein is a product of lipid peroxidation reaction. Formation of free acrolein and its conjugate with lysine residues in oxidized low density lipoproteins. *J Biol Chem* 1998;273:16058–66.
- [4] Requena JR, Fu MX, Ahmed MU, Jenkins AJ, Lyons TJ, Baynes JW, Thorpe SR. Quantification of malondialdehyde and 4-hydroxynonenal adducts to lysine residues in native and oxidized human low-density lipoprotein. *Biochem J* 1997;322:317–25.
- [5] Bolgar MS, Yang CY, Gaskell SJ. First direct evidence for lipid/protein conjugation in oxidized human low density lipoprotein. *J Biol Chem* 1996;271:27999–8001.
- [6] Steinbrecher UP, Zhang HF, Loughheed M. Role of oxidatively modified LDL in atherosclerosis. *Free Radic Biol Med* 1990;9:155–68.
- [7] Haberland ME, Fong D, Cheng L. Malondialdehyde-altered protein occurs in atheroma of Watanabe heritable hyperlipidemic rabbits. *Science* 1988;241:215–8.
- [8] Yla-Herttuala S, Palinski W, Rosenfeld ME, Parthasarathy S, Carew TE, Butler S, Witztum JL, Steinberg D. Evidence for the presence of oxidatively modified low density lipoprotein in atherosclerotic lesions of rabbit and man. *J Clin Invest* 1989;84:1086–95.
- [9] Uchida K, Kanematsu M, Sakai K, Matsuda T, Hattori N, Mizuno Y, Suzuki D, Miyata T, Noguchi N, Niki E, Osawa T. Protein-bound acrolein: potential markers for oxidative stress. *Proc Natl Acad Sci USA* 1998;95:4882–7.
- [10] Maggi E, Chiesa R, Melissano G, Castellano R, Astore D, Grossi A, Finardi G, Bellomo G. LDL oxidation in patients with severe carotid atherosclerosis. A study of in vitro and in vivo oxidation markers. *Arterioscler Thromb* 1994;14:1892–9.
- [11] Salonen JT, Yla-Herttuala S, Yamamoto R, Butler S, Korpela H, Salonen R, Nyyssonen K, Palinski W, Witztum JL. Autoantibody against oxidised LDL and progression of carotid atherosclerosis. *Lancet* 1992;339:883–7.
- [12] Palinski W, Horkko S, Miller E, Steinbrecher UP, Powell HC, Curtiss LK, Witztum JL. Cloning of monoclonal autoantibodies to epitopes of oxidized lipoproteins from apolipoprotein E-deficient mice. Demonstration of epitopes of oxidized low density lipoprotein in human plasma. *J Clin Invest* 1996;98:800–14.
- [13] Uchida K, Osawa T, Hiai H, Toyokuni S. 4-Hydroxy-2-nonenal-trapping ELISA: direct evidence for the release of a cytotoxic aldehyde from oxidized low density lipoproteins. *Biochem Biophys Res Commun* 1995;212:1068–73.

- [14] Ruef J, Hu ZY, Yin LY, Wu Y, Hanson SR, Kelly AB, Harker LA, Rao GN, Runge MS, Patterson C. Induction of vascular endothelial growth factor in balloon-injured baboon arteries. A novel role for reactive oxygen species in atherosclerosis. *Circ Res* 1997;81:24–33.
- [15] Rittner HL, Kaiser M, Brack A, Szweda LI, Goronzy JJ, Weyand CM. Tissue-destructive macrophages in giant cell arteritis. *Circ Res* 1999;84:1050–8.
- [16] Meng J, Sakata N, Takebayashi S, Asano T, Futata T, Nagai R, Ikeda K, Horiuchi S, Myint T, Taniguchi N. Glycoxidation in aortic collagen from STZ-induced diabetic rats and its relevance to vascular damage. *Atherosclerosis* 1998;136:355–65.
- [17] Morisaki N, Kanzaki T, Fujiyama Y, Osawa I, Shirai K, Matsuoka N, Saito Y, Yoshida S. Metabolism of n-3 polyunsaturated fatty acids and modification of phospholipids in cultured rabbit aortic smooth muscle cells. *J Lipid Res* 1985;26:930–9.
- [18] Bailey AL, Southon S. Determination of total long-chain fatty acids in human plasma and lipoproteins, before and during copper-stimulated oxidation, by high-performance liquid chromatography. *Anal Chem* 1998;70:415–9.
- [19] Ruef J, Rao GN, Li F, Bode C, Patterson C, Bhatnagar A, Runge MS. Induction of rat aortic smooth muscle cell growth by the lipid peroxidation product 4-hydroxy-2-nonenal. *Circulation* 1998;97:1071–8.
- [20] Uchida K, Shiraishi M, Naito Y, Torii Y, Nakamura Y, Osawa T. Activation of stress signaling pathways by the end product of lipid peroxidation. 4-Hydroxy-2-nonenal is a potential inducer of intracellular peroxide production. *J Biol Chem* 1999;274:2234–42.
- [21] Leonarduzzi G, Scavazza A, Biasi F, Chiarpotto E, Camandola S, Vogel S, Dargel R, Poli G. The lipid peroxidation end product 4-hydroxy-2,3-nonenal up-regulates transforming growth factor beta1 expression in the macrophage lineage: a link between oxidative injury and fibrosclerosis. *FASEB J* 1997;11:851–7.
- [22] Page S, Fischer C, Baumgartner B, Haas M, Kreusel U, Loidl G, Hayn M, Ziegler-Heitbrock HW, Neumeier D, Brand K. 4-Hydroxynonenal prevents NF-kappaB activation and tumor necrosis factor expression by inhibiting IkappaB phosphorylation and subsequent proteolysis. *J Biol Chem* 1999;274:11611–8.
- [23] Chandra A, Srivastava SK. A synthesis of 4-hydroxy-2-trans-nonenal and 4-(3H) 4-hydroxy-2-trans-nonenal. *Lipids* 1997;32:779–82.
- [24] Srivastava S, Chandra A, Wang LF, Seifert WEJ, DaGue BB, Ansari NH, Srivastava SK, Bhatnagar A. Metabolism of the lipid peroxidation product, 4-hydroxy-trans-2-nonenal, in isolated perfused rat heart. *J Biol Chem* 1998;273:10893–900.
- [25] Shanahan CM, Weissberg PL. Smooth muscle cell heterogeneity: patterns of gene expression in vascular smooth muscle cells in vitro and in vivo. *Arterioscler Thromb Vasc Biol* 1998;18:333–8.
- [26] Bhatnagar A, Liu SQ, Das B, Ansari NH, Srivastava SK. Inhibition kinetics of human kidney aldose and aldehyde reductases by aldose reductase inhibitors. *Biochem Pharmacol* 1990;39:1115–24.
- [27] Siems WG, Grune T, Zollner H, Esterbauer H. Formation and metabolism of the lipid peroxidation product 4-hydroxynonenal in liver and small intestine. In: Poli G, Albano E, Dianzani MU, editors. *Free Radicals: From Basic Sciences to Medicine*. Basel/Switzerland: Birkhaeuser Verlag, 1993:89–101.
- [28] Petras T, Siems WG, Grune T. 4-Hydroxynonenal is degraded to mercapturic acid conjugate in rat kidney. *Free Radic Biol Med* 1995;19:685–8.
- [29] Alin P, Danielson UH, Mannervik B. 4-Hydroxyalk-2-enals are substrates for glutathione transferase. *FEBS Lett* 1985;179:267–70.
- [30] Misra P, Srivastava SK, Singhal SS, Awasthi S, Awasthi YC, Boor PJ. Glutathione S-transferase 8-8 is localized in smooth muscle cells of rat aorta and is induced in an experimental model of atherosclerosis. *Toxicol Appl Pharmacol* 1995;133:27–33.
- [31] Berhane K, Widersten M, Engstrom A, Kozarich JW, Mannervik B. Detoxication of base propenals and other alpha, beta-unsaturated aldehyde products of radical reactions and lipid peroxidation by human glutathione transferases. *Proc Natl Acad Sci USA* 1994;91:1480–4.
- [32] Zimniak P, Singhal SS, Srivastava SK, Awasthi S, Sharma R, Hayden JB, Awasthi YC. Estimation of genomic complexity, heterologous expression, and enzymatic characterization of mouse glutathione S-transferase mGSTA4-4 (GST 5.7). *J Biol Chem* 1994;269:992–1000.
- [33] Grune T, Siems WG, Zollner H, Esterbauer H. Metabolism of 4-hydroxynonenal, a cytotoxic lipid peroxidation product, in Ehrlich mouse ascites cells at different proliferation stages. *Cancer Res* 1994;54:5231–5.
- [34] Srivastava S, Watowich SJ, Petrash JM, Srivastava SK, Bhatnagar A. Structural and kinetic determinants of aldehyde reduction by aldose reductase. *Biochemistry* 1999;38:42–54.
- [35] Dixit BL, Balendiran GK, Watowich SJ, Srivastava S, Ramana KV, Petrash JM, Bhatnagar A, Srivastava SK. Kinetic and structural characterization of the glutathione-binding site of aldose reductase. *J Biol Chem* 2000;275:21587–95.
- [36] Ramana KV, Dixit BL, Srivastava S, Balendiran GK, Srivastava SK, Bhatnagar A. Selective recognition of glutathiolated aldehydes by aldose reductase. *Biochemistry* 2000;39:12172–80.
- [37] Spycher SE, Tabataba-Vakili S, O'Donnell VB, Palomba L, Azzi A. Aldose reductase induction: a novel response to oxidative stress of smooth muscle cells. *FASEB J* 1997;11:181–8.
- [38] Spycher S, Tabataba-Vakili S, O'Donnell VB, Palomba L, Azzi A. 4-Hydroxy-2,3-trans-nonenal induces transcription and expression of aldose reductase. *Biochem Biophys Res Commun* 1996;226:512–6.
- [39] Rittner HL, Hafner V, Klimiuk PA, Szweda LI, Goronzy JJ, Weyand CM. Aldose reductase functions as a detoxification system for lipid peroxidation products in vasculitis. *J Clin Invest* 1999;103:1007–13.
- [40] Iwata T, Sato S, Jimenez J, McGowan M, Moroni M, Dey A, Ibaraki N, Reddy VN, Carper D. Osmotic response element is required for the induction of aldose reductase by tumor necrosis factor-alpha. *J Biol Chem* 1999;274:7993–8001.
- [41] Sellin S, Holmquist B, Mannervik B, Valleo BL. Oxidation and reduction of 4-hydroxyalkenals catalyzed by isozymes of human alcohol dehydrogenase. *Biochemistry* 1991;30:2514–8.
- [42] Allali-Hassani A, Martinez SE, Peralba JM, Vaglenova J, Vidal F, Richart C, Farres J, Pares X. Alcohol dehydrogenase of human and rat blood vessels. Role in ethanol metabolism. *FEBS Lett* 1997;405:26–30.
- [43] Mitchell DY, Petersen DR. The oxidation of alpha-beta unsaturated aldehydic products of lipid peroxidation by rat liver aldehyde dehydrogenases. *Toxicol Appl Pharmacol* 1987;87:403–10.
- [44] Voskoboinik I, Soderholm K, Cotgreave IA. Ascorbate and glutathione homeostasis in vascular smooth muscle cells: cooperation with endothelial cells. *Am J Physiol* 1998;275:C1031–9.
- [45] Eisenbrand G, Schuhmacher J, Golzer P. The influence of glutathione and detoxifying enzymes on DNA damage induced by 2-alkenals in primary rat hepatocytes and human lymphoblastoid cells. *Chem Res Toxicol* 1995;8:40–6.
- [46] Horvath JJ, Witmer CM, Witz G. Nephrotoxicity of the 1:1 acrolein-glutathione adduct in the rat. *Toxicol Appl Pharmacol* 1992;117:200–7.
- [47] Adams JDJ, Klaidman LK. Acrolein-induced oxygen radical formation. *Free Radic Biol Med* 1993;15:187–93.
- [48] Hsu DK, Guo Y, Peifley KA, Winkles JA. Differential control of murine aldose reductase and fibroblast growth factor (FGF)-regulated-1 gene expression in NIH 3T3 cells by FGF-1 treatment and hyperosmotic stress. *Biochem J* 1997;328:593–8.
- [49] Donohue PJ, Alberts GF, Hampton BS, Winkles JA. A delayed-early gene activated by fibroblast growth factor-1 encodes a protein related to aldose reductase. *J Biol Chem* 1994;269:8604–9.